Electrochimica Acta 282 (2018) 64–80

Contents lists available at ScienceDirect

Electrochimica Acta

journal homepage: www.elsevier.com/locate/electacta

# Capacitive properties of novel N-alkyl substituted poly(3,6-dithienyl-9*H*-carbazole)s as redox electrode materials and their symmetric micro-supercapacitor applications

Deniz Yiğit [a, b, *], Mustafa Güllü [a, **]

[a] Department of Chemistry, Faculty of Science, Ankara University, Besevler, 06100, Ankara, Turkey
[b] Department of Basic Pharmaceutical Sciences, Faculty of Pharmacy, Lokman Hekim University, Söğütözü, 06530, Ankara, Turkey

ARTICLE INFO

*Article history:*
Received 8 December 2017
Received in revised form
14 May 2018
Accepted 1 June 2018
Available online 14 June 2018

*Keywords:*
Poly(3,6-dithienylcarbazole)s
Redox electrodes
Capacitive materials
Supercapacitors
Micro-supercapacitors

ABSTRACT

Herein, we present a comparative study about charge storage performances of novel N-alkyl substituted poly(3,6-dithienylcarbazole)-based electrodes for supercapacitor applications. The poly(3,6-dithienylcarbazole) derivatives, poly(9-butyl-3,6-di(thien-2-yl)-9*H*-carbazole) (PTCB), poly(9-hexyl-3,6-di(thien-2-yl)-9*H*-carbazole) (PTCH) and poly(9-octyl-3,6-di(thien-2-yl)-9*H*-carbazole) (PTCO), were electrochemically synthesized for the first time on a metal substrate and directly used as electrode materials in supercapacitor applications. The capacitive performances of PTCB, PTCH and PTCO polymeric films were studied by using cyclic voltammetry, galvanostatic charge/discharge and electrochemical impedance spectroscopy techniques in both three-electrode and real two-electrode micro-supercapacitor device configurations. PTCB, PTCH and PTCO redox-active materials achieved high gravimetric specific capacitances of 147.7, 218.7 and 509.8 F $g^{-1}$, respectively, at a current density of 2.5 mA $cm^{-2}$ in three-electrode cell configurations. Assembled symmetric devices reached maximum specific capacitances of 70.4 (for PTCB), 96 (for PTCH) and 185.5 F $g^{-1}$ (for PTCO). Devices also delivered energy densities of 20.3, 26 and 55 W h $kg^{-1}$ and power densities of 750, 755 and 760 W $kg^{-1}$ with good rate capabilities. Moreover, micro-supercapacitor devices exhibited good long-term cycling stability performances and retained 83.7%, 86.5% and 89.4% of their initial capacitances after 10 000 charge/discharge cycles. The electrochemical performance tests reveal that PTCB, PTCH and PTCO redox-active materials have promising potential to meet requirements of a practical electrochemical energy storage applications.



## 1. Introduction

π-Conjugated organic conducting polymers (CPs) have been receiving more and more attention as electroactive materials with the rapid development in the field of plastic electronics. For the past two decades, CPs have been widely preferred in many different electronic applications including organic photovoltaics (OPVs) [1,2], light emitting diodes (OLEDs) [3,4], electrochromic devices (ECDs) [5,6], organic field effect transistors (OFETs) [7], smart windows [8], sensors [9], and artificial muscles [10] due to their excellent electronic and optoelectronic properties. Recently, CPs have attracted great interest as redox-active capacitive materials in supercapacitors, also known as ultracapacitors [11–14].

Supercapacitors are considered as next generation alternative electrochemical energy storage systems and located between batteries and traditional dielectric capacitors with regard to their power and energy densities [15]. Supercapacitors also possess many desirable features such as high charge storage capacity, short charging time, cycling life performance, good operational safety and eco-friendliness for effective energy storage systems [16–18]. It is widely accepted that electrode material is the most decisive component on capacitive performance of a supercapacitor. The physical and electronic properties of an electroactive material, such as surface morphology, thickness, electrical conductivity, internal resistance and durability, directly affect the performance of supercapacitors. Hence, great majority of researchers have paid

* Corresponding author. Department of Basic Pharmaceutical Sciences, Faculty of Pharmacy, Lokman Hekim University, Söğütözü, 06530, Ankara, Turkey
** Corresponding author.
*E-mail addresses:* dyigit@science.ankara.edu.tr, deniz.yigit@lokmanhekim.edu.tr (D. Yiğit), gullu@ankara.edu.tr (M. Güllü).

https://doi.org/10.1016/j.electacta.2018.06.005
0013-4686/

attention to develop new and more effective electrode materials possessing unique electrochemical and morphological features [19,20].

Carbonaceous materials (carbon nanotubes, carbon nanofibers, graphenes and carbon aerogels) [21–26], transition metal oxides ($V_2O_5$, $SnO_2$, NiO, $MnO_2$, $TiO_2$ and $RuO_2$) [27–32] and π-conjugated conducting polymer derivatives [19] have been widespreadly utilized as electroactive materials in fundamental supercapacitor researches and commercial applications, so far. Carbon-based electrode materials basically store electrical charges and release energy by means of a physical sorption/desorption mechanism, akin to traditional dielectric capacitors [33]. It is expected that carbonaceous materials can reach high capacitance and energy density values because of their wider surface area and porous structures, and display excellent chemical and mechanical strength and fast ion kinetics which are regarded as desirable morphological and electronic properties for an ideal electrode material. Nevertheless, their capacitive efficiency is limited by the binding process of electrode preparation [34]. On the other hand, as being distinctively different from carbonaceous materials, transition metal oxide- and conducting polymer-based electrode materials make use of quick and reversible Faradaic redox process for charge storage in addition to electrostatic interactions at the electrode/electrolyte interface. Owing to supplementary Faradaic reactions, metal oxides and conducting polymers can store and provide 10–100 times greater amount of electrical charge compared to carbon-based electrode materials [35,36]. Nevertheless, many transition metal oxides suffer from main limitations such as low electrical conductivity, limited surface area, poor electron transfer ability, high cost and toxicity. These disadvantages are the primary obstacles facing metal oxide-based practical supercapacitor applications [37]. As for π-conjugated conducting polymers, they have considerable superiorities with relatively suitable surface morphology, better flexibility properties, unlimited structural diversity and applicability, environmental stability and friendliness, lower fabrication costs, excellent electronic conductivities and higher redox capacitances compared to metal oxide-based materials [38]. Futhermore, conducting polymers switch very quickly between their two extreme redox states. The fast switching feature, generally known as doping/dedoping process, gives the conducting polymer-based electrode materials the ability to fairly short charging time, which makes conducting polymers better choices for supercapacitor applications. Moreover, electrochemical synthesis methods allow directly deposition of conducting polymer films on the different current collector substrate surfaces without the need of any polymeric binder [39].

Up to the present, a wide variety of conducting polymers including polythiophenes (PTh), polyanilines (PANI), polypyrroles (PPy), poly(3,4-ethylenedioxythiophene) (PEDOT) and polycarbazoles (PCbz) derivatives have been prepared and broadly applied as redox-active capacitive materials in various symmetric and asymmetric supercapacitors [15,40–47]. The electrode materials based on PTh, PANI, PPy, PEDOT and PCbz have delivered specific capacitance values between 33 and 640 $F\,g^{-1}$ in various two- and three-electrode cell configurations. Although conducting polymer electrodes have satisfactory energy storage performances and superior electrochemical or morphological properties, almost all of them suffer remarkable physical degradation. This mechanical instability arises from the repeated shrinking and swelling movements on the conducting polymer backbone during the Faradaic charge/discharge (doping/dedoping) processes [48]. To alleviate cycling stability problem and improve long-term charge/discharge characteristics of the conducting polymer-based electrodes, various strategies have been put forward in recent years since poor cycling stability greatly restricts applicability of polymeric capacitive materials in supercapacitors. [49–52] Our previously published studies have revealed that the reasonable design of novel conducting polymer derivatives can be considered as alternative and effective tool to improve long-term cycling life of polymer-based redox-active materials [47]. For instance, the novel poly(-thiophene) be more specific derivatives containing carbazole moiety were able to better tolerate the mechanical degradation caused by volume change on redox-active polymeric surface during the repeated redox cycles owing to the high mechanical strenght and stability of carbazole units. High specific capacitance and energy density values over a broad potential range have been also observed for these poly(3,6-dithienylcarbazole)-based film electrodes as well as remarkable long-term cycling performance enhancement.

In this context, we basically focus on the preparation of novel conducting polymer derivatives to address the problem of low cycle life based on mechanical instability on the polymer-based electrodes. As well known, polycarbazole (PCbz) derivatives exhibit high mechanical strength and flexibility during Faradaic redox reactions, as well as their easy formation of stable radicals and high hole-transporting abilities [53,54]. Therefore, poly(carbazole)s can buffer the volume changes originated from the swelling and shrinkage movements and undergo mechanical degradation less. Based on this property of polycarbazole derivatives, it was aimed that long-term cycling performance of redox-active materials could be improved by introducing carbazole units into conducting polymer backbones. For this purpose, novel N-substituted poly(3,6-dithienylcarbazole) derivatives, poly(9-butyl-3,6-di(thien-2-yl)-9*H*-carbazole) (PTCB), poly(9-hexyl-3,6-di(thien-2-yl)-9*H*-carbazole) (PTCH) and poly(9-octyl-3,6-di(thien-2-yl)-9*H*-carbazole) (PTCO) have been electrochemically synthesized by direct coating on the stainless steel substrates and employed as redox-active materials in this work. Apart from the attempts to improve the long-term life cycle, novel 3,6-dithienylcarbazole monomers were derivatized with butyl-, hexyl- and octyl- homologous alkyl groups *via* their nitrogen atoms so as to investigate the effect of alkyl chain length over the surface morphology and capacitive performance of polymeric redox-active materials. Previous work by our research group has put forth that terthiophene-based conducting polymer films containing different alkyl side chains exhibited disparate morphological structures [55]. In the light of preliminary studies, it was expected to create a change in morphological properties of poly(3,6-dithienylcarbazole)-based polymeric networks by altering alkyl pendant groups on conducting polymer backbones. Depending on the morphological diversity, it was aimed to obtain different redox capacitance values with these redox-active polymeric materials. Redox characteristics and charge storage performances of poly(9-butyl-3,6-di(thien-2-yl)-9*H*-carbazole) (PTCB), poly(9-hexyl-3,6-di(thien-2-yl)-9*H*-carbazole) (PTCH) and poly(9-octyl-3,6-di(thien-2-yl)-9*H*-carbazole) (PTCO)-based redox active electrode materials were evaluated by cyclic voltammetry (CV) and galvanostatic charge/discharge (GCD) studies with a standard three-electrode cell configuration. Moreover, p-p type symmetrical micro-supercapacitor cells were also assembled by utilizing PTCB, PTCH and PTCO coated stainless steel substrates. Capacitive performance tests of micro-supercapacitor devices were performed by cyclic voltammetry (CV), galvanostatic charge/discharge (GCD) and electrochemical impedance spectroscopy (EIS) techniques under a two-electrode system with an operating voltage of 1.5 V.

## 2. Experimental

### 2.1. Materials

Carbazole, tetrakis(triphenylphosphine)palladium (0) and 2-

(tributylstannyl)thiophene were purchased from Sigma-Aldrich. Stainless steel substrate (dimension of 0.4 mm thickness, 1 cm width and 1 cm length) was commercially available and employed as a current collector after chemical etching process. 3,6-Dibromo-9H-carbazole was prepared according to previously reported synthetic procedure [56]. Solvent (acetonitrile, ACN) and supporting electrolyte (tetrabutylammonium tetrafluoroborate, $Bu_4NBF_4$) used in electrochemical studies were dried using appropriate methods and stored under an inert atmosphere. The silver wire employed as an $Ag/Ag^+$ pseudo-reference electrode was carefully calibrated versus $Fc/Fc^+$ ferrocene redox couple (0.3 V).

### 2.2. Synthesis of monomers

N-alkyl substituted 3,6-dithienyl-9H-carbazole derivatives (**TCB**, **TCH** and **TCO**) were synthesized step by step as follows; (*i*) 3,6-dibromo-9H-carbazole (**2**) was initially obtained following a similar reaction conditions to previously reported $SiO_2$-supported dibromination method, (*ii*) then, nucleophilic substitution reactions were performed in the presence of a strong base under single-mode microwave irradiation for the synthesis of N-alkyl substituted 3,6-dibromo-9*H*-carbazole derivatives (**6,7,8**), (iii) thiophene units were finally attached to N-alkylcarbazole ring system through the palladium-catalyzed Stille cross-coupling reaction to form the 3,6-dithienyl-9H-carbazole monomer backbone (Scheme 1). FTIR, $^1H$ NMR, $^{13}C$ NMR, mass spectroscopy and elemental analysis techniques were used for the structural analyses of novel carbazole-based monomers (**TCB**, **TCH** and **TCO**). The details of experimental studies and spectral characterization data can be shown in the supporting information document.

### 2.3. Determination of redox behaviour of monomers and preparation of polymer-based electrode materials

Using a typical cyclic voltammetry (CV) technique in between 0.0 V and 2.0 V potential range, redox characteristics of carbazole-based monomers (**TCB**, **TCH** and **TCO**) and oxidation/reduction potentials of resulting conducting polymer films (**PTCB**, **PTCH** and **PTCO**) were determined in the first stage of electrochemical studies. Cyclic voltammograms were recorded using a three-electrode cell configuration (platinum disc working and auxiliary electrodes and silver wire $Ag/Ag^+$ pseudo-reference electrode) with 150 mV $s^{-1}$ scan rate under ambient conditions. 0.1 M solution of $Bu_4NBF_4$ in ACN was used as the supporting electrolyte solution for all CV studies. Single scan cycle voltammetry technique was also performed to explore redox properties of **PTCB**, **PTCH** and **PTCO** conducting polymer films in both anodic and cathodic regions. Single scan cyclic voltammograms were scanned between 0.0 V and 2.0 V and −2.5 V and 0.0 V using **PTCB**, **PTCH** and **PTCO** coated platinum disc electrodes in the monomer free electrolytic medium at scan rate of 150 mV $s^{-1}$.

After obtaining sufficient data about redox characteristics of **TCB**, **TCH** and **TCO** monomers, **PTCB**, **PTCH** and **PTCO** conducting polymer films were potentiostatically deposited on stainless steel substrates (SS) at suitable monomer oxidation potentials. A potentiostatic technique was prefered in particular for preparation of **PTCB**, **PTCH** and **PTCO** coated SS electrode materials so as to control the mass loading of active material on the SS substrates. Constant potential electrolyses were executed with chemically etched SS working electrodes, SS auxiliary electrodes and an $Ag/Ag^+$ pseudo-reference silver wire electrode at 1.81 V for **TCB**, 1.84 V for **TCH** and 1.87 V for **TCO** in the presence of 0.05 M monomer concentration in 0.1 M $Bu_4NBF_4$/ACN solution under nitrogen atmosphere. Following the coating of conducting polymer layers, **PTCB**, **PTCH** and **PTCO**-based electrode materials were electrochemically neutralized at −0.35 V for 150 s to provide the charge balance. Then, the prepared **PTCB**, **PTCH** and **PTCO** films were repeatedly rinsed with ACN to clean out electrolyte residues and unreacted monomers from polymeric network. Finally, the redox-active electrode materials were kept under vacuum at 60 °C for 2.5 h and dried by removing the solvent. The chemical structure characterizations of **PTCB**, **PTCH** and **PTCO** polymeric materials were realized by FTIR. Scanning electron microscopy (SEM) was used to probe the morphological properties of **PTCB**, **PTCH** and **PTCO** redox-active layers on SS substrates. The mass of **PTCB**, **PTCH** and **PTCO** electrochemically grown on SS substrates were determined using a microanalytical balance ($\Delta = \pm 0.01$ mg). The average of six parallel weightings was taken as total redox-active material mass and used in calculations of both three-electrode and two-electrode cell configuration. The average active material loading on each electrode was measured to be approximately 1.20 mg $cm^{-2}$.

***Poly(9-butyl-3,6-di(thien-2-yl)-9H-carbazole) (PTCB):*** IR (ATR) $\nu$/ $cm^{-1}$ 3068 (w, aromatic C—H strecthing), 2938, 2875 (w, aliphatic C—H strecthing), 1639 (m, polyconjugation aromatic —C═C- strecthing), 1430, 1368, 1285 (m, aliphatic C—H bending), 1215, 1136 (s, —C—O— strecthing).

***Poly(9-hexyl-3,6-di(thien-2-yl)-9H-carbazole) (PTCH):*** IR (ATR) $\nu$/ $cm^{-1}$ 3065 (w, aromatic C—H strecthing), 2940, 2869 (w, aliphatic C—H strecthing), 1640 (m, polyconjugation aromatic —C═C- strecthing), 1432, 1371, 1280 (m, aliphatic C—H bending), 1218, 1142 (s, —C—O— strecthing).

***Poly(9-octyl-3,6-di(thien-2-yl)-9H-carbazole) (PTCO):*** IR (ATR) $\nu$/ $cm^{-1}$ 3086 (w, aromatic C—H strecthing), 2965, 2886 (w, aliphatic C—H strecthing), 1639 (m, polyconjugation aromatic —C═C- strecthing), 1432, 1365, 1288 (m, aliphatic C—H bending), 1218, 1138 (s, —C—O— strecthing).

### 2.4. Fabrication of symmetrical type micro-supercapacitors

p-p Type symmetrical micro-supercapacitor devices were simply constructed by sandwiching two conducting polymer coated SS substrates for electrochemical performance tests. **PTCB**, **PTCH** and **PTCO**-based redox-active materials were employed as both positive and negative electrodes in two-electrode cell configuration. Firstly, **PTCB**, **PTCH** and **PTCO** modified electrode materials were kept for 1.5 h in 0.5 M $Bu_4NBF_4$/ACN supporting electrolyte solution to ensure good wetting. Then, two conducting polymer-based redox-active electrodes were brought together and separated by an electrolyte-soaked filter paper (Whatman Grade 1 filter paper, 15 mm diameter). Finally, modified electrode materials were carefully assembled by overlapping and two-electrode setup was wrapped with a thin paraffin band to seal against environmental conditions. Configuration of package micro-supercapacitor devices are symbolized as below;

**Device I:** PTCB-based electrode/ separator paper soaked to 0.5 M $Bu_4NBF_4$/ACN/ PTCB-based electrode (PTCB//PTCB)
**Device II:** PTCH-based electrode/ separator paper soaked to 0.5 M $Bu_4NBF_4$/ACN/ PTCH-based electrode (PTCH//PTCH)
**Device III:** PTCO-based electrode/ separator paper soaked to 0.5 M $Bu_4NBF_4$/ACN/ PTCO-based electrode (PTCO//PTCO)

### 2.5. Evaluation of supercapacitive performances

All three-electrode measurements were performed using conducting polymer coated SS working and auxiliary electrodes (**PTCB**, **PTCH** and **PTCO**) and a silver wire $Ag/Ag^+$ pseudo-reference electrode in 0.5 M $Bu_4NBF_4$/ACN supporting electrolyte solution at room temperature. Supercapacitor performance tests of

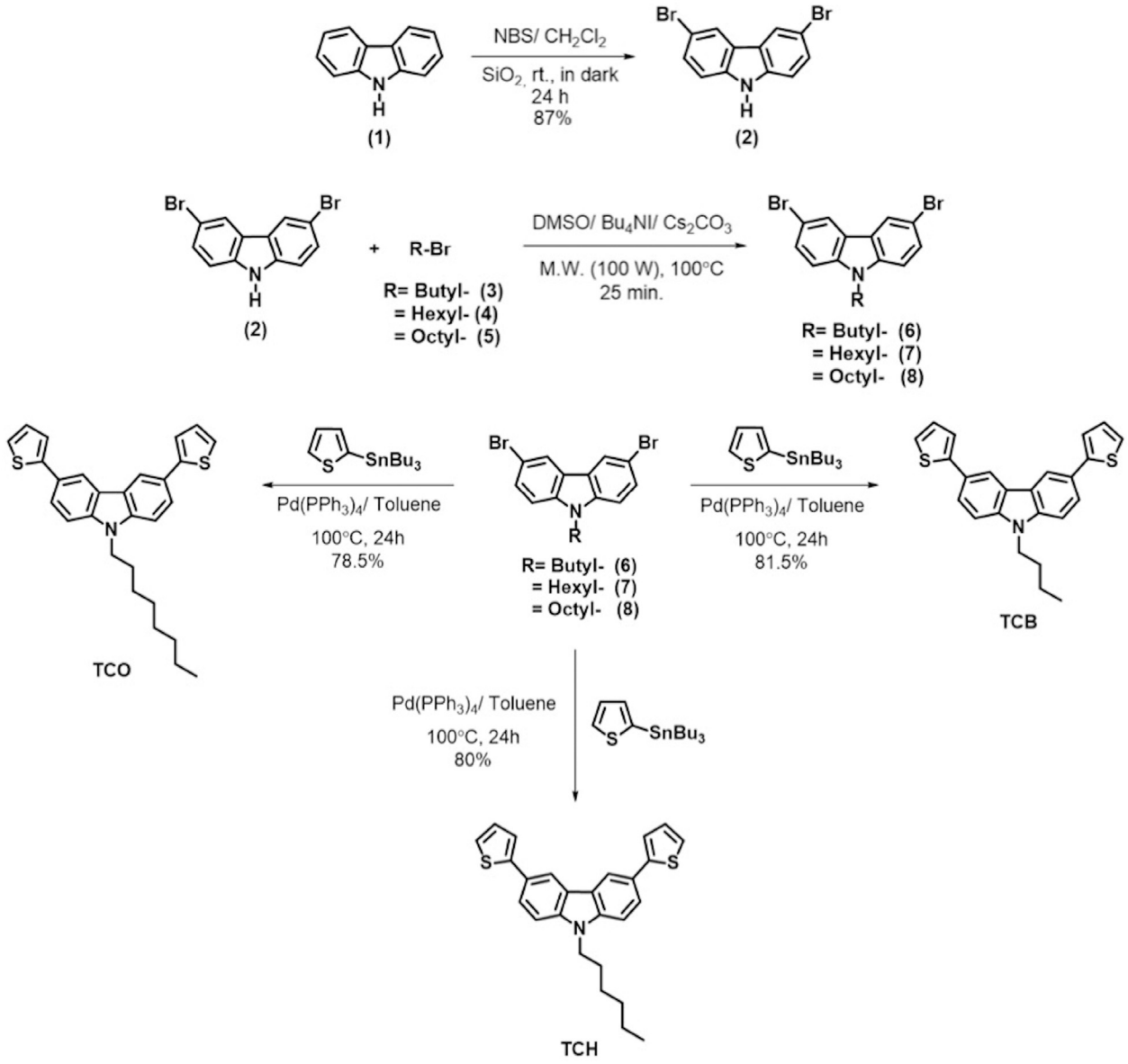


**Scheme 1.** Synthetic procedure for 3,6-dithienyl-9*H*-carbazole monomers, **TCB**, **TCH** and **TCO**.

symmetrical micro-supercapacitor devices (Device I, Device II and Device III) were directly carried out by connecting the lead of auxiliary and reference to the same modified SS electrode. Cyclic voltammetry (CV) was used to evaluate the current-potential (I-V) profiles. Cyclic voltammograms were recorded from 0.0 V to 1.5 V with scan rates of 10, 25, 50, 100, 150 and 250 mV $s^{-1}$. Charge/discharge behaviors were tested by constant current charge/discharge technique (GCD) at various constant current densities (2.5, 4.5, 6.5, 8.5, 10.5, 12.5 mA $cm^{-2}$) over a potential range of 1.5 V. For determination of long-term cycle lifes of micro-supercapacitor devices, typical GCD curves were recorded between 0.0 V and 1.5 V at 2.5 mA $cm^{-2}$ constant current density over 10 000 charge/discharge cycles. Electrochemical impedance spectroscopy (EIS) measurements were carried out in the frequency range from 10 000–0.01 Hz under a DC applied voltage of 0.0 V with a voltage amplitude of 5 mV rms. Gravimetric specific capacitances ($C_{spec}$), energy densities ($E$) and power densities ($P$) were calculated using GCD curves based on following equations, respectively;

$$C_{spec} = (I \times td)/(\Delta V \times m_{ac}) \quad (1)$$

$$E = \left[C_{spec} \times (\Delta V)^2\right] \Big/ 7.2 \quad (2)$$

$$P = (3600 \times E)/t_d \quad (3)$$

where I and $t_d$ are the discharge current (mA) and discharge time (s), respectively. ΔV corresponds to the potential range including the IR drop value during the discharge process ($V_{max}$ − IR drop) (V) while $m_{ac}$ describes the total mass of redox-active material present only on working electrode for three-electrode configuration and on both electrodes for two-electrode device setup (mg).

### 2.6. Equipments and instrumentation

Microwave-assisted reactions were conducted with a CEM

Discover S-Class single-mode microwave instrument under 100 W microwave irradiation. Column chromatography studies were performed with $SiO_2$ 60 (0.063–0.200 mm) using analytical grade solvents. $^1$H NMR and $^{13}$C NMR spectra were recorded using Varian-Mercury 400 MHz (FT)-NMR spectrometer at room temperature. Chemical shifts ($\delta$) are given in ppm relative to tetramethylsilane (TMS). FTIR spectra were recorded on a Perkin-Elmer Spectrum 100 spectrometer (ATR mode). IR absorptions were reported in $cm^{-1}$. Mass spectra were collected by Water 2695 Alliance Micromass ZQ LC/MS using a direct inlet probe and Agilent Technologies 6890 N Network GC System/5975B VL MSD at an ionization potential (EI) of 70 eV. Element analyses were performed on a Leco CHNS-932 elemental analyser. The morphological properties of polymeric samples on SS substrates were probed by a Zeiss Ultra Plus FE-SEM and Zeiss EVO 40 500 V to 30 kV. All electrochemical measurements were either carried out using a Princeton Applied Research PAR-2273 potentiostat/galvanostat or a Radiometer VoltaLab PST050 potentiostat/galvanostat-high voltage booster 100 HVB100.

## 3. Results and discussion

This study had two main motivations as mentioned earlier. Firstly, long-term cycling lifes of thiophene-based redox-active materials were expected to be increased by incorporating

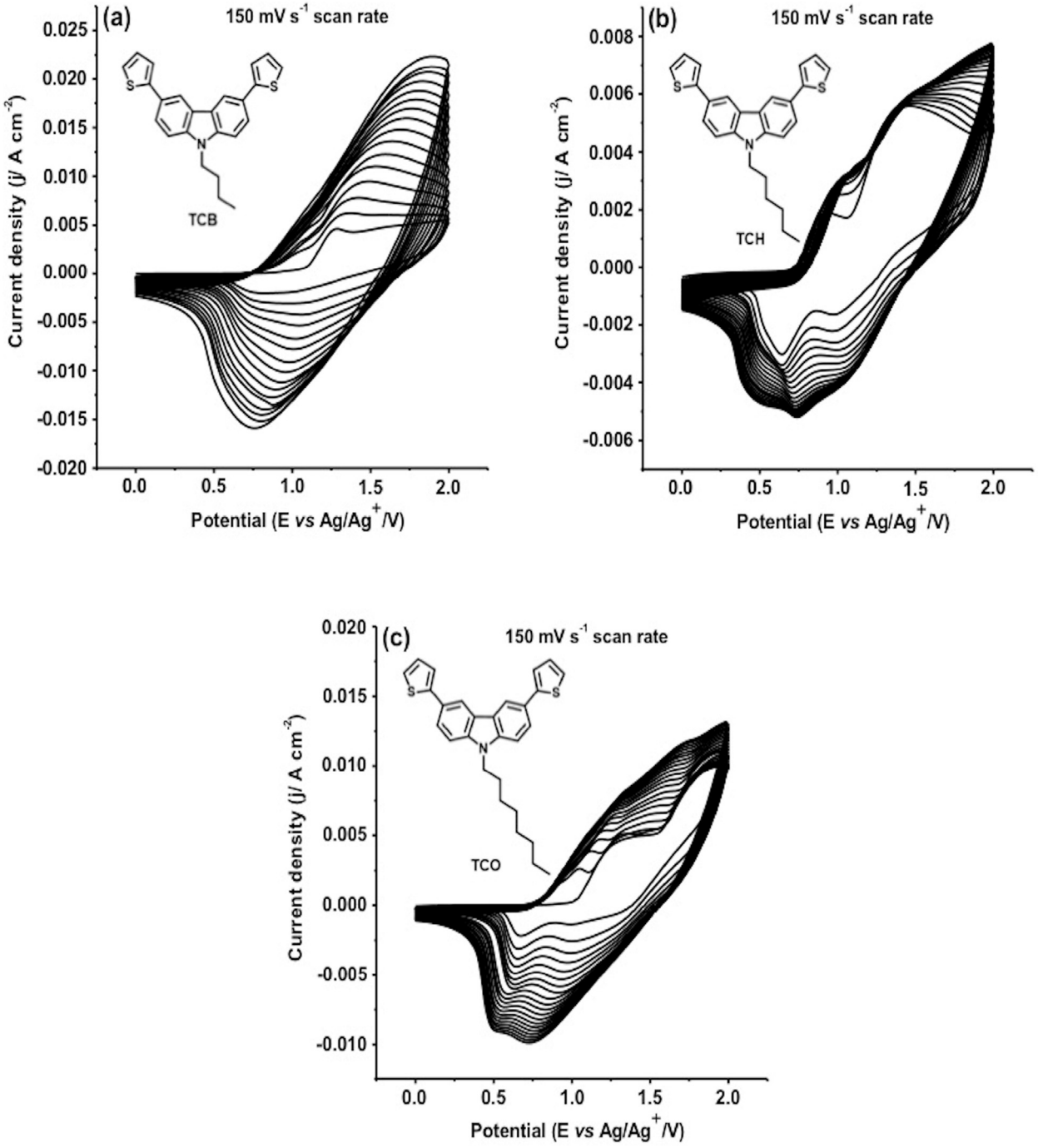


**Fig. 1.** Typical electropolymerization CV curves of (a) **TCB**, (b) **TCH** and (c) **TCO** monomers in 0.1 M $Bu_4NBF_4$/ACN at 150 mV $s^{-1}$ scan rate.

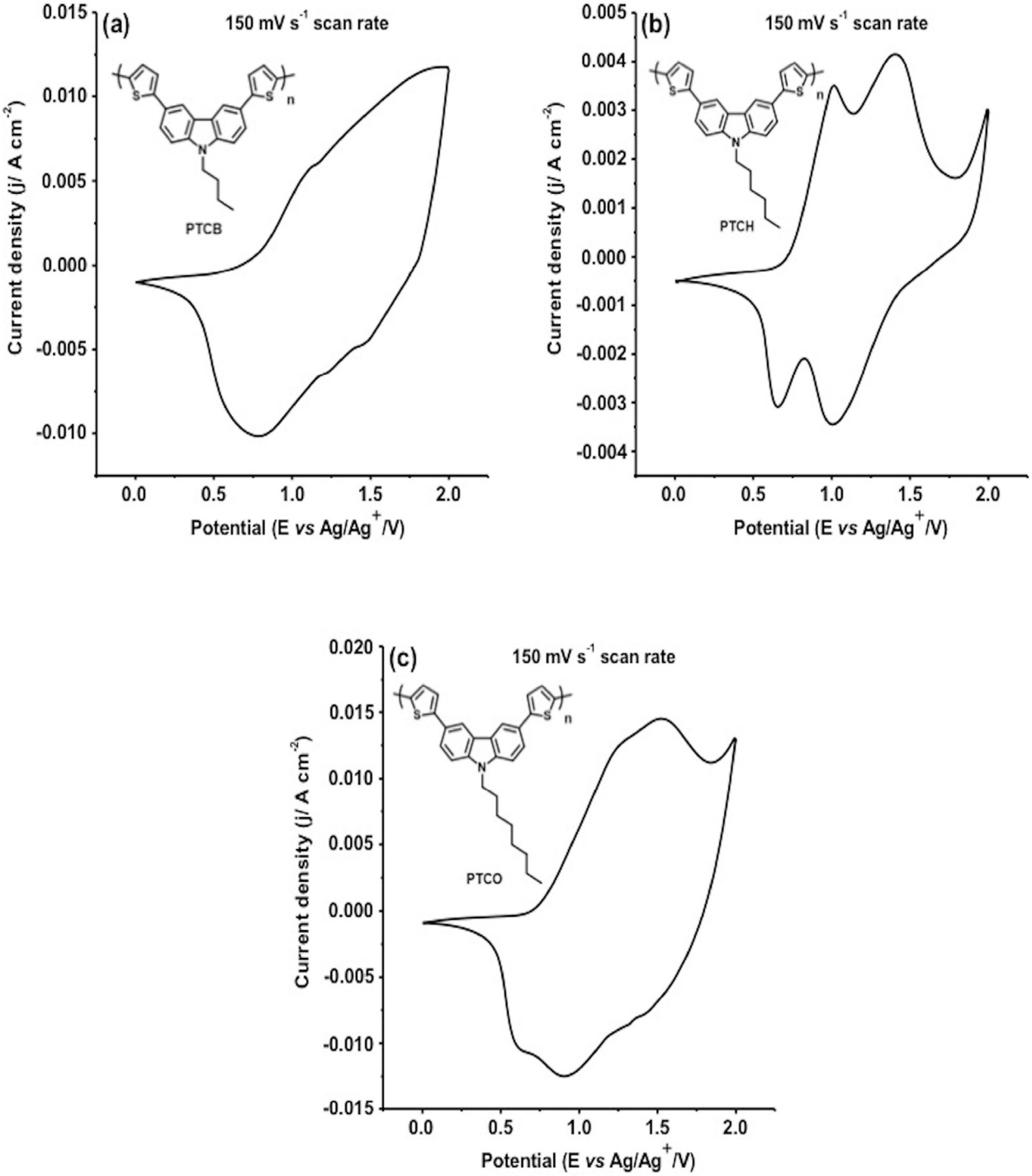


**Fig. 2.** Anodic single scan CV curves of (a) **PTCB**, (b) **PTCH** and (c) **PTCO** polymeric films in 0.1 M $Bu_4NBF_4$/ACN at a scan rates of 150 mV $s^{-1}$ in monomer-free solution.

heteroaromatic structures, known to have a good mechanical strength and stable under reactive conditions, into conducting polymer backbone. Secondly, our goal was to create a difference on the surface properties of conducting polymer networks by derivatizing the main skeleton with different pendant analogue groups. By taking these two points into account, novel N-alkyl substituted 3,6-dithienyl-9*H*-carbazole monomers, 9-butyl-3,6-di(thien-2-yl)-9*H*-carbazole (**TCB**), 9-hexyl-3,6-di(thien-2-yl)-9*H*-carbazole (**TCH**) and 9-octyl-3,6-di(thien-2-yl)-9*H*-carbazole (**TCO**), were synthesized in three steps, as illustrated in Scheme 1.

Typical anodic electropolymerization behaviours were observed in cyclic voltammetry for **TCB**, **TCH** and **TCO** monomers, recorded between 0.0 V and 2.0 V potential window at 150 mV $s^{-1}$ scan rate (Fig. 1a–c). In the first anodic scans, all samples exhibited characteristic irreversible monomer oxidation peaks. These peaks were observed at 1.81 V for **TCB**, 1.84 V for **TCH** and 1.87 V for **TCO**, respectively. Quite small differences between oxidation potentials of monomers can be associated with steric hindrances of alkyl chains. Octyl- pendant group creates a more pronounced steric effect than those of butyl- and hexyl- chains in terms of molecular

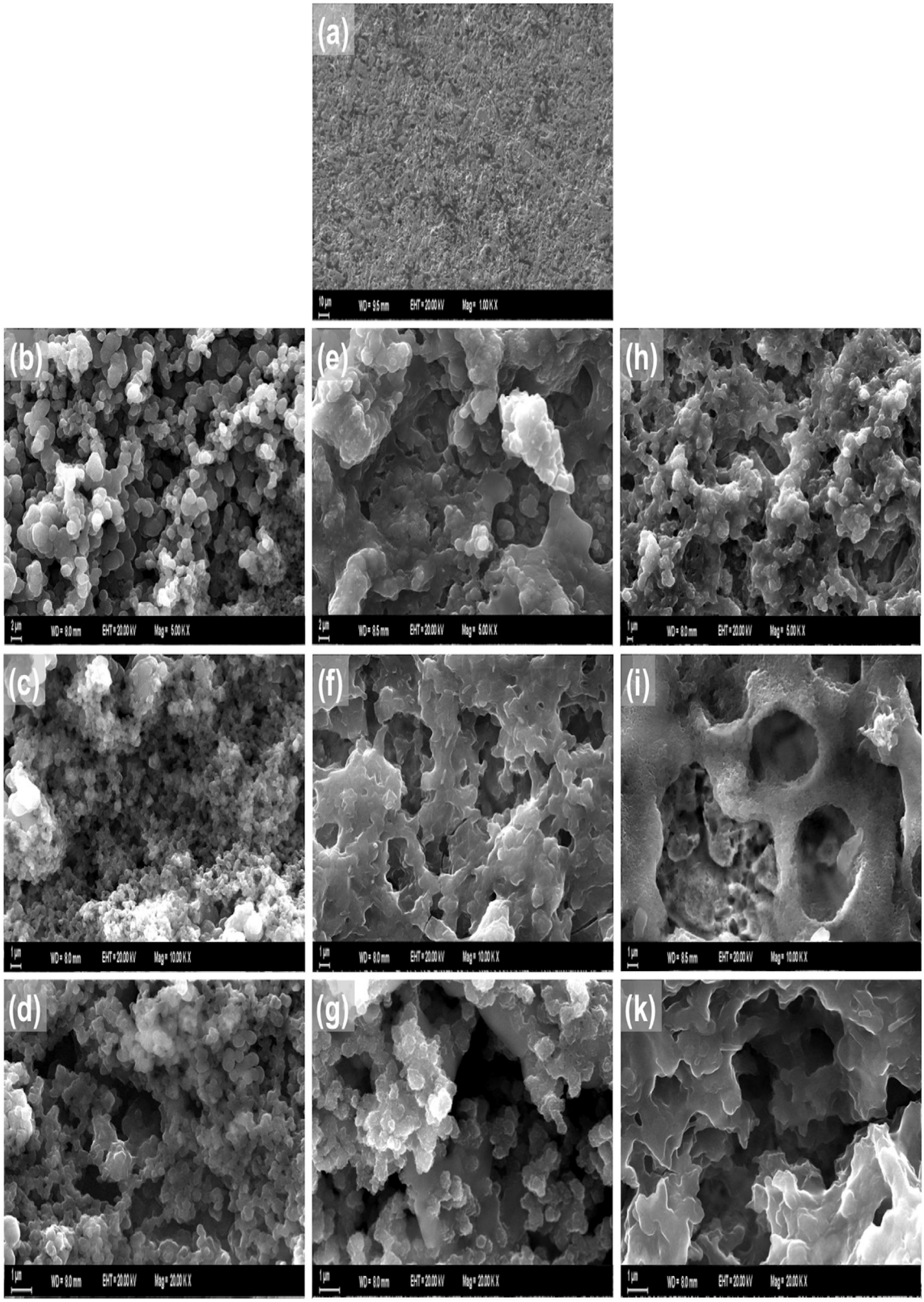


**Fig. 3.** Top-view SEM images of (a) bare SS substrate, (b–d) **PTCB**, (e–g) **PTCH** and (h–k) **PTCO** polymeric films on SS electrodes at different magnifications.

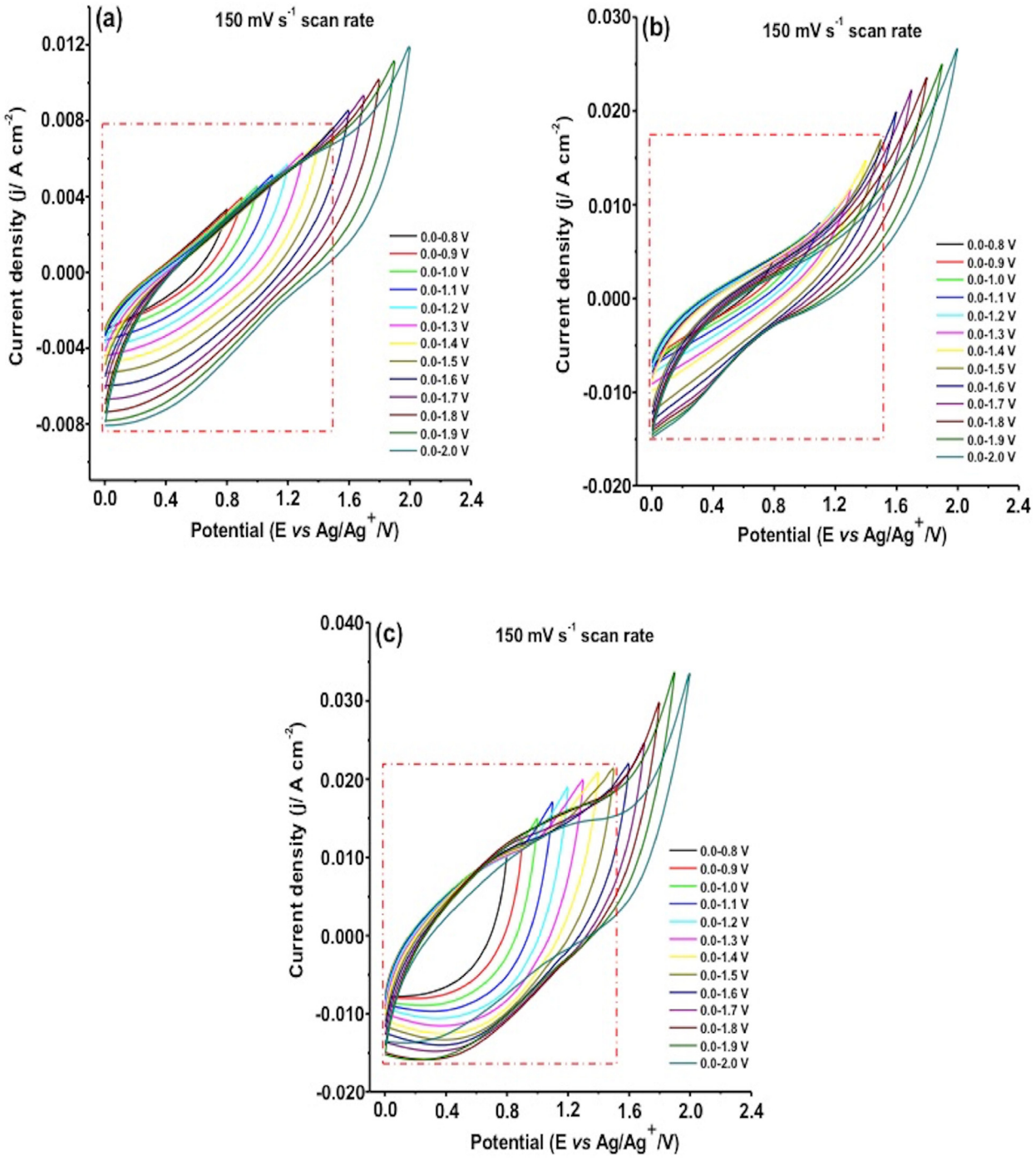


**Fig. 4.** CV curves of (a) **PTCB**, (b) **PTCH** and (c) **PTCO** redox-active materials as positive electrodes in different operating potential range in 0.5 M $Bu_4NBF_4$/ACN at 150 mV $s^{-1}$ scan rate.

planarity and monomer mobility [57–60]. Owing to this effect, **TCO** monomer could approach electrode surface more difficult for electron transfer and got oxidized at a relatively slightly higher positive potential than **TCB** and **TCH**.

As seen from Fig. 1a–c, oxidation peaks of monomers were accompanied by new reversible polymer redox couples with a progressive increase in the current density after first cycles. 2nd and 3rd cycles of cyclic voltammograms resulted in rapid formation of **PTCB**, **PTCH** and **PTCO** conducting polymer films on the platinum working electrodes. Resulting **PTCH** and **PTCO** films markedly exhibited two reversible redox waves during repeated oxidation/reduction cycles due to different polaronic species originating from both thiophene and carbazole heteroaromatic systems. These reversible redox couples were centered at 1.04 V/ 0.65 V and 1.43 V/ 0.98 V for **PTCH** and 1.15 V/ 0.67 V and 1.46 V/ 0.99 V for **PTCO**, respectively. On the other hand, a broad reversible oxidation/reduction peak was observed at 1.41 V/ 1.10 V for **PTCB** film because of a possible overlapping two different redox couples on each other, as can be shown in Fig. 1a.

p- and n-doping properties of **PTCB**, **PTCH** and **PTCO** films were

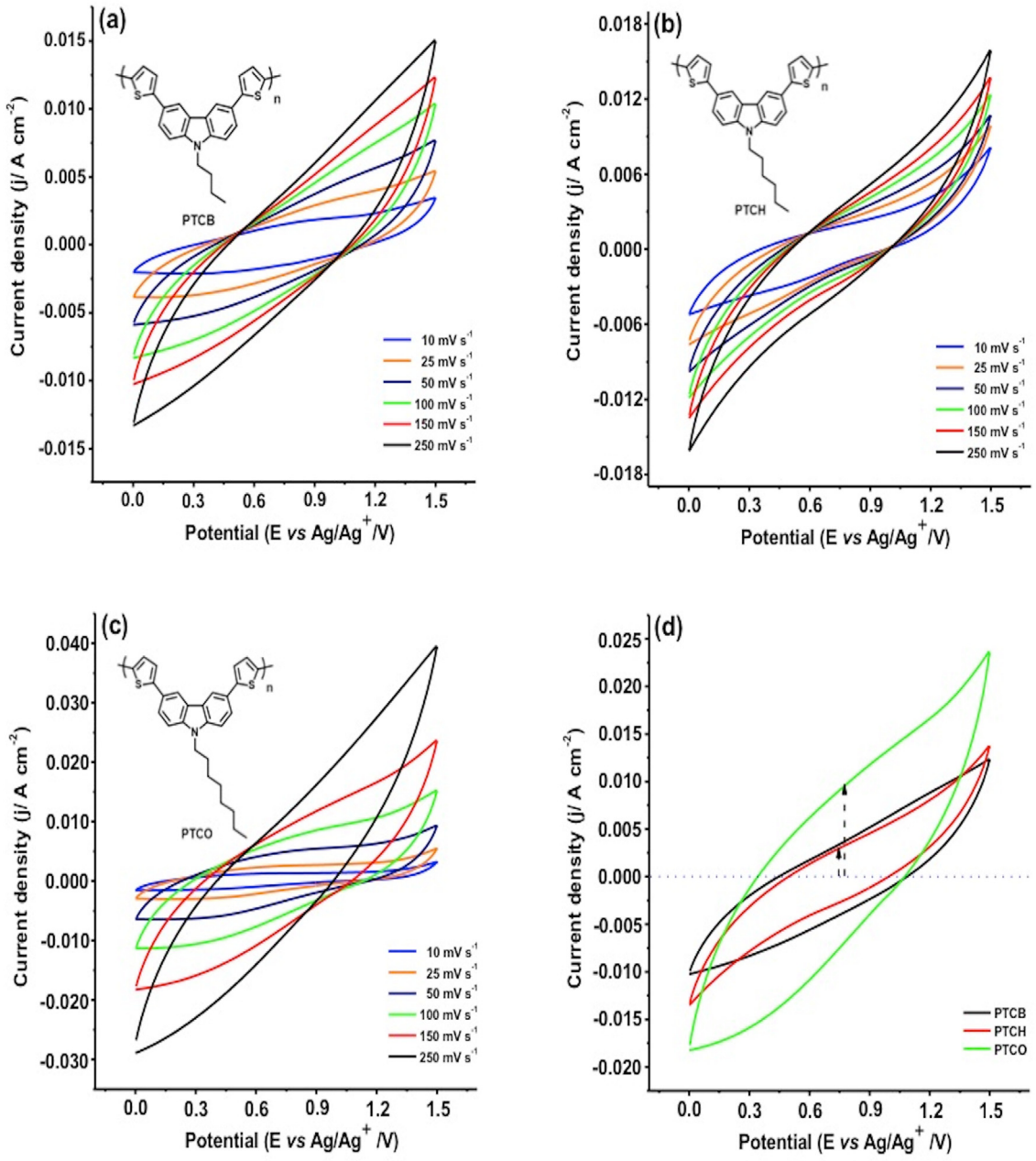


**Fig. 5.** Redox behaviors of (a) **PTCB**, (b) **PTCH**, (c) **PTCO**-based electrodes in 0.5 M $Bu_4NBF_4$/ACN at various scan rates (10–250 mV $s^{-1}$) and (d) comparative normalized CV curves of redox-active materials at 150 mV $s^{-1}$ in three-electrode cell configuration.

also investigated by recording single scan cyclic voltammograms in a monomer-free electrolytic media. Single scan CV results reveal that all conducting polymer films had a tendency to show only *p*-dopable behaviors (Fig. 2a–c). As expected, **PTCH** and **PTCO** demonstrated two reversible p-doping and their corresponding *p*-dedoping characteristics. These reversible oxidation/reduction peak potentials were determined to be 1.01 V/ 0.65 V and 1.40 V/ 1.00 V for **PTCH** and 1.25 V/ 0.64 V and 1.52 V/ 0.92 V for **PTCO** *vs*. Ag wire pseudo-reference electrode. **PTCB** exhibited broad p-doping peak between 1.15 V and 1.51 V and dedoping peak at 0.77 V with a different tendency from **PTCH** and **PTCO**. The cathodic scans between 0.0 V and − 2.5 V for **PTCB**, **PTCH** and **PTCO** conducting polymer films are given in Fig. S4 (see supporting information document).

After examination of the redox behaviors of **TCB**, **TCH** and **TCO** and their resulting conducting polymers (**PTCB**, **PTCH** and **PTCO**) by CV, these electroactive monomers were electrochemically polymerized and deposited on stainless steel (SS) current collectors to prepare polymeric electrode materials. In the preparation procedure, constant potential electrolysis technique was used under the same conditions to control the loading of the electroactive material per current collector substrates, which allows to make an objective comparison in capacitive performance evaluations of polymeric films. The grown conducting polymer layers on SS substrates (**PTCB**, **PTCH** and **PTCO**) were chemically characterized with FTIR results. The morphological properties of polymeric films were observed by using scanning electron microscopy (SEM). When the top-view SEM observations obtained for bare and modified SS substrates are compared (Fig. 3), it can be clearly seen **PTCB**, **PTCH** and **PTCO** films homogeneously coated across the SS surfaces. SEM

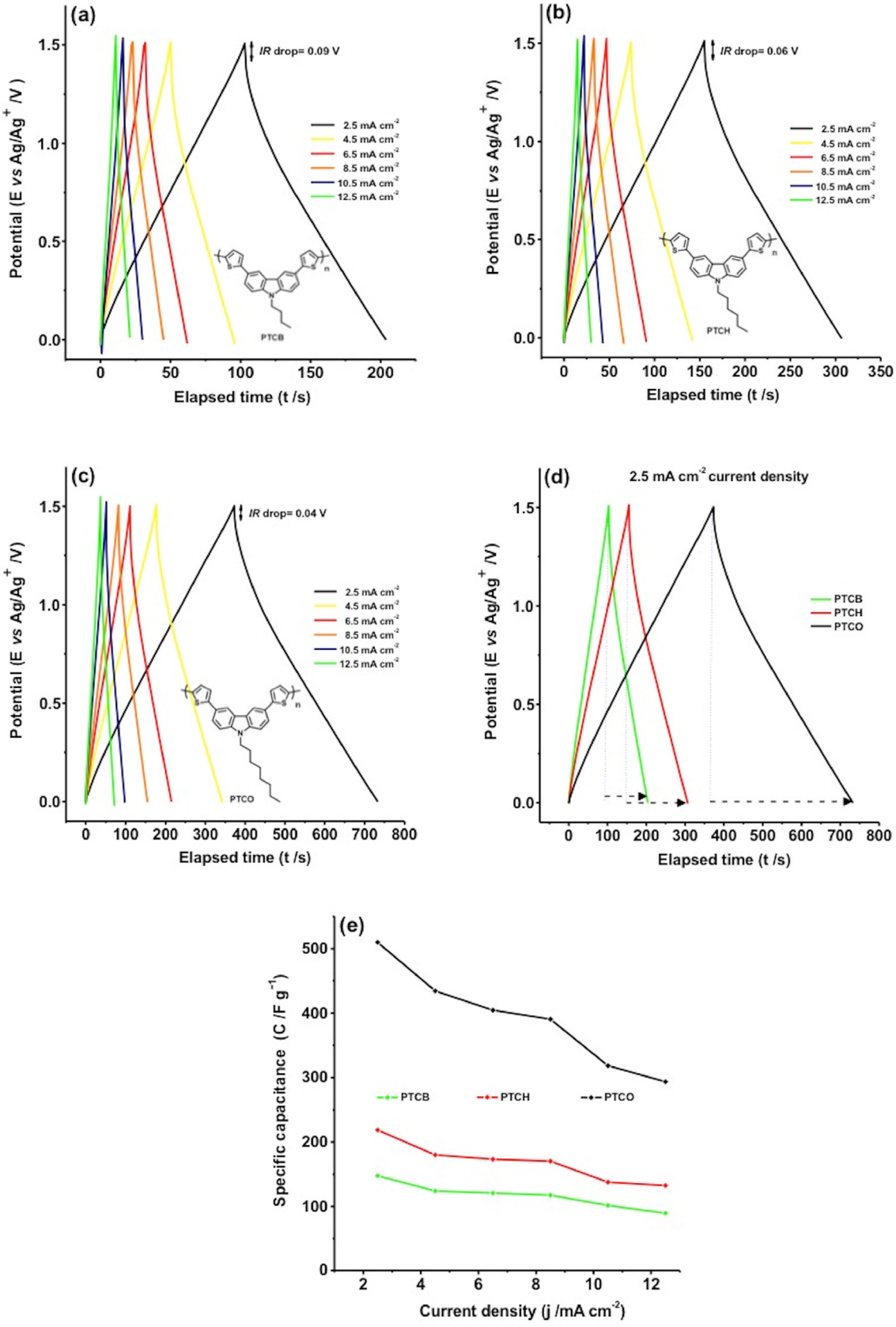


**Fig. 6.** GCD curves of (a) **PTCB**, (b) **PTCH**, (c) **PTCO** redox-active materials electrodes at 2.5, 4.5, 6.5, 8.5, 10.5 and 12.5 mA $cm^{-2}$ current densities, (d) comparative GCD curves at 2.5 mA $cm^{-2}$ and (e) specific capacitance changes of electrode materials under different current densities.

images at different magnifications in Fig. 3b–k further confirmed that **PTCB**, **PTCH** and **PTCO** polymeric layers have different morphological properties. For example, **PTCB** film presents a characteristic cauliflower-like morphological structure while **PTCH** and **PTCO** films exhibit spongy-like three-dimensional network structures (Fig. 3b, e and 3h). As can be understood from SEM observations, the length of pendant alkyl chains on conducting polymer backbones resulted in a significant difference on surface morphologies of polymer films, as expected. This appreciable morphological difference from **PTCB** to **PTCO** film might be attributed to the solubility and mobility of pendant alkyl chains since electropolymerization studies for all samples were conducted under the same conditions. Octyl- and hexyl- chains are better soluble pendant groups compared to butyl- chain. Hence, prolongation of alkyl chain decreases the mobility of side group due to intense van der Waals interactions between alkyl chains. This provides the formation of a more ordered polymeric network by enabling the growth of oligomeric or polymeric chains in a certain direction during electropolymerization process (Fig. 3e–k). Conversely, as can be shown in Fig. 3b–d, **PTCB** polymeric network exhibited an agglomerated morphological structure due to self-aggregation caused by the low solubility of the shorter alkyl pendant groups (butyl- chains). On the basis of SEM observations, it can be said that the spongy-like three-dimensional structures of **PTCH** and **PTCO** networks can ensure more effective and plentiful ion diffusion pathways to enhance their charge storage performances, as expected. On the other hand, the agglomerated structure of **PTCB** films may create a barrier effect against ions movements and penetrations on the polymeric network.

Prior to charge storage performance measurements, ideal operating potential range for all redox-active electrodes was identified by recording typical CV curves at 150 mV $s^{-1}$ constant scan rate in various potential scales of a wide range (0.0 V and 2.0 V) in a symmetrical three-electrode setup. The representative cyclic voltammograms in Fig. 4a–c indicate that no significant increase was observed in CV currents of **PTCB**, **PTCH** and **PTCO** redox-active films after 1.5 V. In the light of preliminary CV studies, the window of 0.0 V and 1.5 V was defined as ideal working potential range for electrochemical performance tests.

The first performance evaluation of **PTCB**, **PTCH** and **PTCO** redox-active materials was performed in a three-electrode system to make a direct comparison of electrochemical features regardless of different variables. The current-potential (I-V) profiles of **PTCB**, **PTCH** and **PTCO** electrodes in Fig. 5 exhibited shuttle-like shapes, as predicted. The I-V profiles in ideal double-layer capacitors are nearly rectangular and mirror-image shape since current density is independent of applied potential to supercapacitor device during discharge process [22]. But, CV profiles of conducting polymer-based electrode materials generally present deviations from rectangular-like shape due to the pseudocapacitive effect resulted from Faradaic redox reactions (doping/dedoping processes) as well as pure electrochemical double-layer [39]. On the other hand, Fig. 5d clearly reveals that higher redox current density and larger normalized CV area were obtained for **PTCO** film compared with both **PTCB** and **PTCH**, indicating **PTCO** electrode have better pseudocapacitive charge storage performance than those of **PTCB** and **PTCH**. CV studies for **PTCB**, **PTCH** and **PTCO** were also conducted with different scan rates to explore the dependence of redox behaviors of polymeric film electrodes on scan rate. Generally, ion diffusion rate in the conducting polymer matrix is slow at high scan rates. This leads to a fading of the charge/discharge characteristic of redox-active materials and a deformity in the CV profiles. As can be seen in Fig. 5a–c, **PTCB**, **PTCH** and **PTCO**-based electrodes still kept their shapes of the I-V profiles as scan rate was gradually increased from 10 mV $s^{-1}$ to 250 mV $s^{-1}$. This response demonstrates that **PTCB**, **PTCH** and **PTCO** redox-active materials have fast and reversible redox behavior and high-rate charge/discharge performance even at high scan rates during Faradaic processes.

GCD studies were carried out over a potential scale of 0.0 V and 1.5 V at various constant current densities to make a more comprehensive performance assessment about charge storage capacities of polymer-based electrodes. Fig. 6a–c show characteristic charge/discharge curves at 2.5 mA $cm^{-2}$ for prepared **PTCB**, **PTCH** and **PTCO**-based redox-active electrodes, in which it can be clearly seen that all samples exhibited a charge/discharge profile close to triangular shape. This good symmetry in GCD curves means that **PTCB**, **PTCH** and **PTCO** films have highly reversible and well balanced Faradaic charge storage behaviors, closer to an ideal supercapacitive character. Also, very small IR-drop (ohmic drop) values were observed for **PTCB** (IR-drop = 0.09 V), **PTCH** (IR-drop = 0.06 V) and **PTCO** (IR-drop = 0.04 V) at 2.5 mA $cm^{-2}$ current density during galvanostatic cycling between 0.0 V and 1.5 V,

**Table 1**
Capacitive performances of different redox-active electrode materials.

| Redox-active material | Working potential range | Electrolytic media | Specific capacitance ($C_{spec}$) | Ref. |
|---|---|---|---|---|
| PEDOT | - 0.5–0.9 V | 0.1 M $NaClO_4$ | 176 F $g^{-1}$ at 0.75 mA $cm^{-2}$ | [42] |
| Poly(EDOTbithiophene-EDOT) | 0.0–1.0 V | 0.1 M $Bu_4NPF_6$/ACN | 171 F $g^{-1}$ at 1 A $g^{-1}$ | [43] |
| Poly(2-(thiophene-2-yl)furan) | 0.1–1.1 V | 0.1 M $LiClO_4$/ACN | 392 F $g^{-1}$ at 5 A $g^{-1}$ | [44] |
| PEDOT/PSS | - 0.8–0.8 V | 0.5 M $Na_2SO_4$ | 334 F $g^{-1}$ at 0.5 A $g^{-1}$ | [45] |
| Poly(3′,4′-dibutoxy-2,2′:5′,2″-ter thiophene) | 0.0–1.6 V | 0.5 M $Bu_4NBF_4$/ACN | 94.3 F $g^{-1}$ at 2.5 mA $cm^{-2}$ | [55] |
| Poly(3′,4′-bis(hexyloxy)-2,2′:5′,2″-ter thiophene) | 0.0–1.6 V | 0.5 M $Bu_4NBF_4$/ACN | 227.3 F $g^{-1}$ at 2.5 mA $cm^{-2}$ | [55] |
| Poly(3′,4′- bis(octyloxy)-−2,2′:5′,2″-ter thiophene) | 0.0–1.6 V | 0.1 M $Bu_4NBF_4$/ACN | 443 F $g^{-1}$ at 2.5 mA $cm^{-2}$ | [55] |
| Poly(thiophene) | - 0.6–0.8 V | 1 M $Na_2SO_4$ | 103 F $g^{-1}$ at 0.3 A $g^{-1}$ | [61] |
| Poly(pyrrole) | - 0.6–0.6 V | $H_3PO_4$/PVA | 170 F $g^{-1}$ at 0.5 A $g^{-1}$ | [62] |
| Poly(aniline) | 0.0–1.0 V | PVSA | 98 F $g^{-1}$ at 20 mA | [63] |
| Poly(3-methylthiophene) | 1.15–2.0 V | 1 M $Et_4NBF_4$/PC | 220 F $g^{-1}$ at 0.3 A $g^{-1}$ | [64] |
| Poly(4,4′-dipent oxy-2,2′:5′,2″-ter thiophene) | - 0.27–1.03 V | 1 M $Et_4NBF_4$/PC | 190 F $g^{-1}$ | [65] |
| Poly(4-methyl-3,4-dihydrothieno[3,4b] [1,4]oxazine) | 0.0–1.0 V | 0.1 M $Bu_4NBF_4$/ACN | 312.3 F $g^{-1}$ at 1 mA $cm^{-2}$ | [66] |
| Poly(4-ethyl-3,4-dihydrothieno[3,4b] [1,4]oxazine) | 0.0–0.85 V | 0.5 M $Bu_4NBF_4$/ACN | 325.1 F $g^{-1}$ at 1 mA $cm^{-2}$ | [66] |
| **PTCB** | **0.0 – 1.5 V** | **0.5 M $Bu_4NBF_4$/ACN** | **147.7 F $g^{-1}$ at 2.5 mA $cm^{-2}$** | **This work** |
| **PTCH** | **0.0 – 15 V** | **0.5 M $Bu_4NBF_4$/ACN** | **218.7 F $g^{-1}$ at 2.5 mA $cm^{-2}$** | **This work** |
| **PTCO** | **0.0 – 1.5 V** | **0.5 M *Bu*$_4$$NBF_4$/ACN** | **509.8 F $g^{-1}$ at 2.5 mA $cm^{-2}$** | **This work** |

Bold indicates Novel redox-active electrode materials used in this study.

indicating low internal resistances in the redox-active electrode materials.

The gravimetric specific capacitances ($C_{spec}$) for a single electrode material were measured taking into account GCD curves recorded at 2.5 mA $cm^{-2}$ current density. **PTCB**, **PTCH** and **PTCO** redox-active electrode materials delivered 147.7, 218.7 and 509.8 F $g^{-1}$ gravimetric specific capacitance values, respectively. As can be understood from these results, **PTCO** redox-active material exhibited an attractive supercapacitive performance compared to **PTCB**- and **PTCH**-based electrodes. Mainly, better charge storage performance of **PTCO** electrode can be attributed to its suitable morphology. It seems that the 3D spongy-like network structure of **PTCO** film provided more charge storage capacity by increasing the ion diffusion pathways and transporting of supporting electrolyte ions, as expected. Promoted by this property, **PTCO** redox-active electrode achieved higher specific capacitance than those of **PTCB** and **PTCH**. From the other side, it can be concluded that agglomerated morphological structure of **PTCB** polymeric network restricted ion diffusion mechanisms and Faradaic redox reactions by creating a barrier effect against ion mobility in comparison with 3D spongy-like structures of **PTCH** and **PTCO** redox-active films. **PTCB**, **PTCH** and **PTCO** redox-active materials reached higher and comparable gravimetric specific capacitances to many other conducting polymer-based pseudocapacitive electrode materials (Table 1).

GCD curves for **PTCB**, **PTCH** and **PTCO** electrodes were also

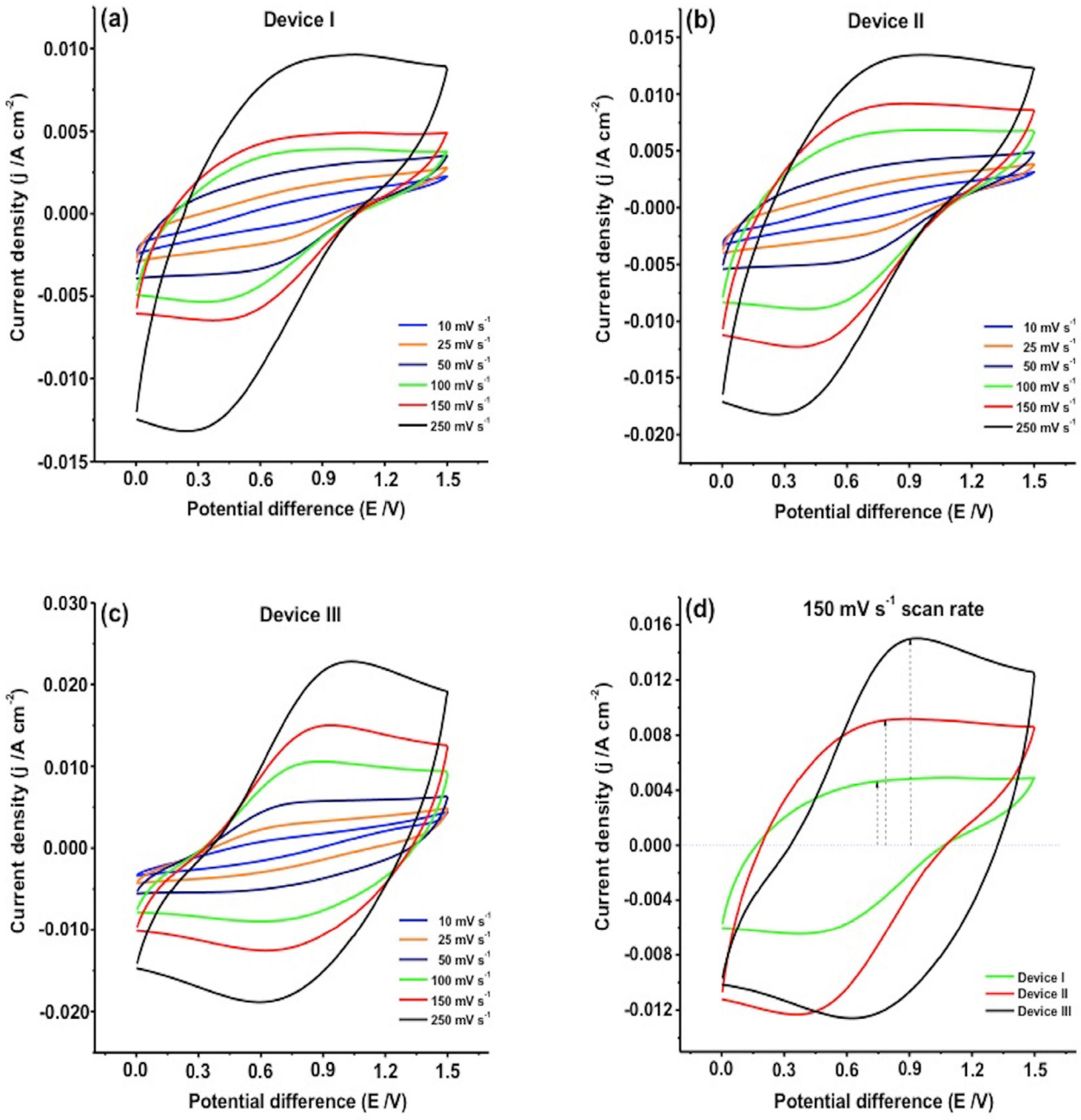


**Fig. 7.** I–V profiles of (a) Device I, (b) Device II, (c) Device III symmetric micro-supercapacitor devices at various scan rates and (d) Device I, Device II and Device III at a scan rate of 150 mV $s^{-1}$.

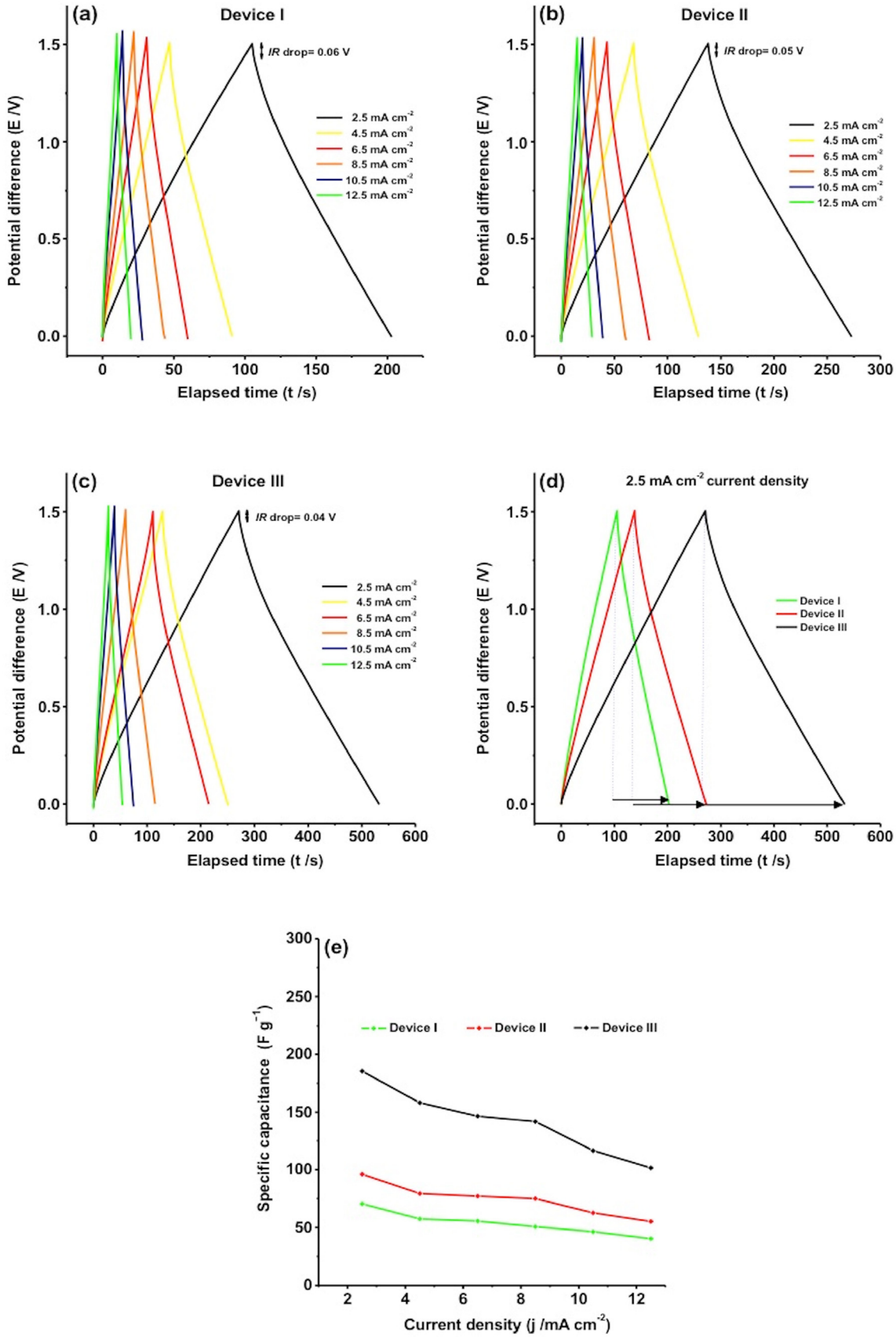


**Fig. 8.** GCD curves of (a) Device I, (b) Device II, (c) Device III, (d) comparative GCD curves at 2.5 mA $cm^{-2}$ and (e) specific capacitance changes of electrode materials under different current densities.

recorded at various current densities different from 2.5 mA $cm^{-2}$ to elucidate the relationship between applied current density and charge storage performance. Current density is a directly influencing parameter on the capacitive behavior. At higher discharge current densities, GCD curves not only present a symmetry distortion, but also the specific capacitance decreases dramatically due to the increase in IR-drop value caused by the limited ion diffusion rates and doping/dedoping redox reactions. Fig. 6a–c demonstare that **PTCB**, **PTCH** and **PTCO** redox-active electrode materials were able to maintain up to 60% of their initial specific capacitances over the potential range of 0.0 V–1.5 V in spite of a 5-fold increase in current density (from 2.5 mA $cm^{-2}$ to 12.5 mA $cm^{-2}$). The dependence of specific capacitance values on applied current densities was plotted in Fig. 6e. These results confirm that **PTCB**, **PTCH** and **PTCO**-based electrodes have good rate capabilities and fast charge transfer abilities, indicating they are promising redox materials for practical energy storage applications.

After characterization of redox behaviors of **PTCB**, **PTCH** and **PTCO**-based electrode materials, the supercapacitive performances of polymeric redox-active materials in a real supercapacitor setups were also examined in two-electrode systems. It is well known that two-electrode test system greatly differs from three-electrode cell configuration in terms of offering several benefits in different aspects. Specific capacitance, energy or power density values can be measured for the whole cell in two-electrode setup whereas these parameters can be calculated for only single electrode (working electrode) in the case of three-electrode cell configuration. In two-electrode system, the potential difference across counter electrode can be also controlled on account of the fact that the potential applied to supercapacitor cell is divided almost equally by both the working and the counter electrode. If an assessment is made regarding above advantages, it can be said that more precise and realistic results of the performance evaluations are obtained with a two-electrode setup. Assembled by using **PTCB**, **PTCH** and **PTCO** coated SS substrates as symmetrical p-p type setup, micro-supercapacitor devices (Device I, Device II and Device III, respectively) were initially characterized through CV at 10–250 mV $s^{-1}$ scan rates. All micro-supercapacitor devices exhibited I-V profiles relatively closer to rectangular shapes compared to the I-V profiles in the three-electrode configuration (Fig. 7a–c), as expected from a typical two-electrode measurement. CV curves of the micro-supercapacitor devices could maintain their shapes of I-V profiles by incrementally increases in scan rate. Based on the redox current densities and normalized CV areas in the comparative cyclic voltammograms in Fig. 7d, it can also be clearly understood that Device III exhibited better pseudocapacitive performance than Device I and Device II. The CV studies performed with two-electrode devices further endorse that **PTCB**, **PTCH** and **PTCO** materials have fast and reversible redox behavior and good rate charge/discharge ability.

GCD profiles were recorded at different constant current densities (2.5, 4.5, 6.5, 8.5, 10.5 and 12.5 mA $cm^{-2}$) to determine charge/discharge behaviors and calculate capacitive performance parameters for micro-supercapacitor devices, in the potential range of 0.0 V and 1.5 V. The reflection of good rate capability properties, fast charge transfer kinetics and low internal resistances of **PTCB**, **PTCH** and **PTCO**-based electrode materials on the device performances can be clearly seen in Fig. 8a–c. Device I, Device II and Device III micro-supercapacitors presented nearly symmetric GCD profiles with tolerable IR-drop values (IR-drop = 0.06 V for Device I, IR-drop = 0.05 V for Device II and IR-drop = 0.04 V for Device III) at 2.5 mA $cm^{-2}$, just like in three-electrode measurements. Besides, Device I, Device II and Device III underwent an average loss of 43% in their gravimetric capacitances with a 5-fold increase in the current density (Fig. 8e). GCD results obtained from micro-supercapacitor device measurements are in good agreement with three-electrode characterizations. Fig. 8d depicts the comparative GCD curves of solid-state micro-supercapacitors. As clearly seen from Fig. 8d, Device III exhibited longer discharging duration at 2.5 mA $cm^{-2}$ current density than discharge durations of Device I and Device II, again reveals that **PTCO** redox-active material has a better charge storage capacity compared to **PTCB** and **PTCH**. Gravimetric specific capacitance ($C_{spec}$), energy density (E) and power density (*P*) values were calculated for solid-state micro-supercapacitor devices by utilizing from these GCD curves at 2.5 mA $cm^{-2}$ current density, and the results are summed up in Table 2.

**Table 2**
Specific capacitance, energy and power density values of micro-supercapacitor devices.

| Micro-supercapacitor device | Specific capacitance ($C_{spec}$) F $g^{-1}$ | Energy density (E) W h $kg^{-1}$ | Power density (P) W $kg^{-1}$ |
|---|---|---|---|
| Device I | 70.4 | 20.3 | 750 |
| Device II | 96 | 28 | 755 |
| Device III | 185.5 | 55 | 760 |

Apart from specific capacitance, energy and power density values, the long-term cycling performance is considered to be an another essential parameter for real energy storage applications. Evaluation of the long-term cycling life of solid-state micro-supercapacitor devices was also performed by typical GCD studies at 2.5 mA $cm^{-2}$ current density in a potential window of 1.5 V over 10 000 cycles and the resulting specific capacitance changes were plotted as a function of cycle numbers in Fig. 9. In the cycling life tests, Device I, Device II and Device III demonstrated good cycling performances and preserved 83.7% (from 70.4 to 58.9 F $g^{-1}$), 86.5% (from 96 to 83 F $g^{-1}$) and %89.4 (from 185.5 to 165.8 F $g^{-1}$) of their

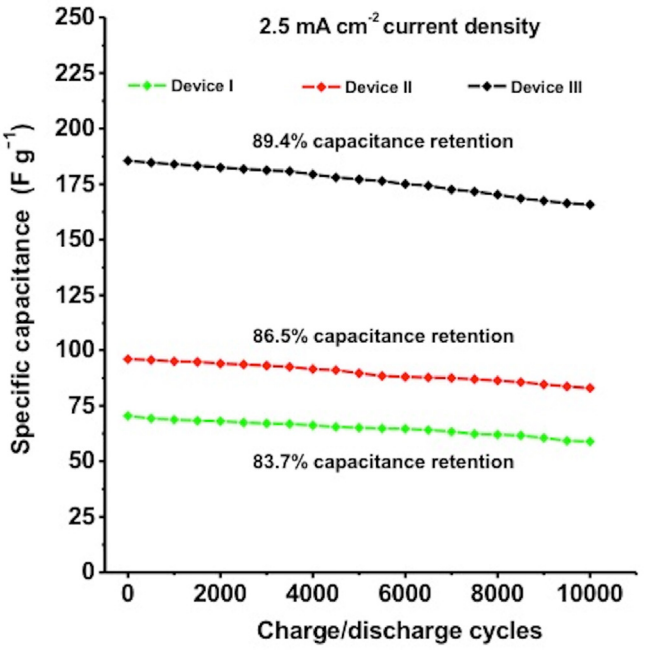


**Fig. 9.** Long-term cycling life performances of Device I Device II and Device III micro-supercapacitor devices at 2.5 mA $cm^{-2}$ current density over 10 000 charge/discharge cycles.

initial charge storage capacities, respectively, after 10 000 cycles.

These capacitance retention values indicate **PTCB**, **PTCH** and **PTCO** redox-active materials possess very stable charge/discharge cycle lifes. Also, good long-term cycling stability performances obtained for Device I, Device II and Device III micro-supercapacitors are very competitive in comparison with reported various polythiophene-, polypyrrole- and polyaniline-based supercapacitor applications in the literature [19,61,67–69]. Device III, on the other hand, was able to cope with the surface degradation caused by volumetric changes and diffusion resistance on polymeric film electrode better than Device I and Device II under the same conditions, as observed from Fig. 9. Such superior cycling performance can be attributed to the morphological properties of **PTCO** polymeric network. As excepted from 3D spongy-like structure, it could provide more preferable access channels for diffusion of electrolyte ions. Lower diffusion resistance would bring along a better cycling performance for **PTCO** redox-active material during long-term charge/discharge cycles, as predicted. Based on all the information obtained by these results, it can be concluded that the design and synthesis of novel conducting polymer derivatives has a very promising potential to overcome cycle life defect of conducting polymers in supercapacitor use and fabricate more effective redox-active electrode materials with excellent long-term cycling performances.

Device I, Device II and Device III were finally studied by EIS in order to get comprehensive information about electronic

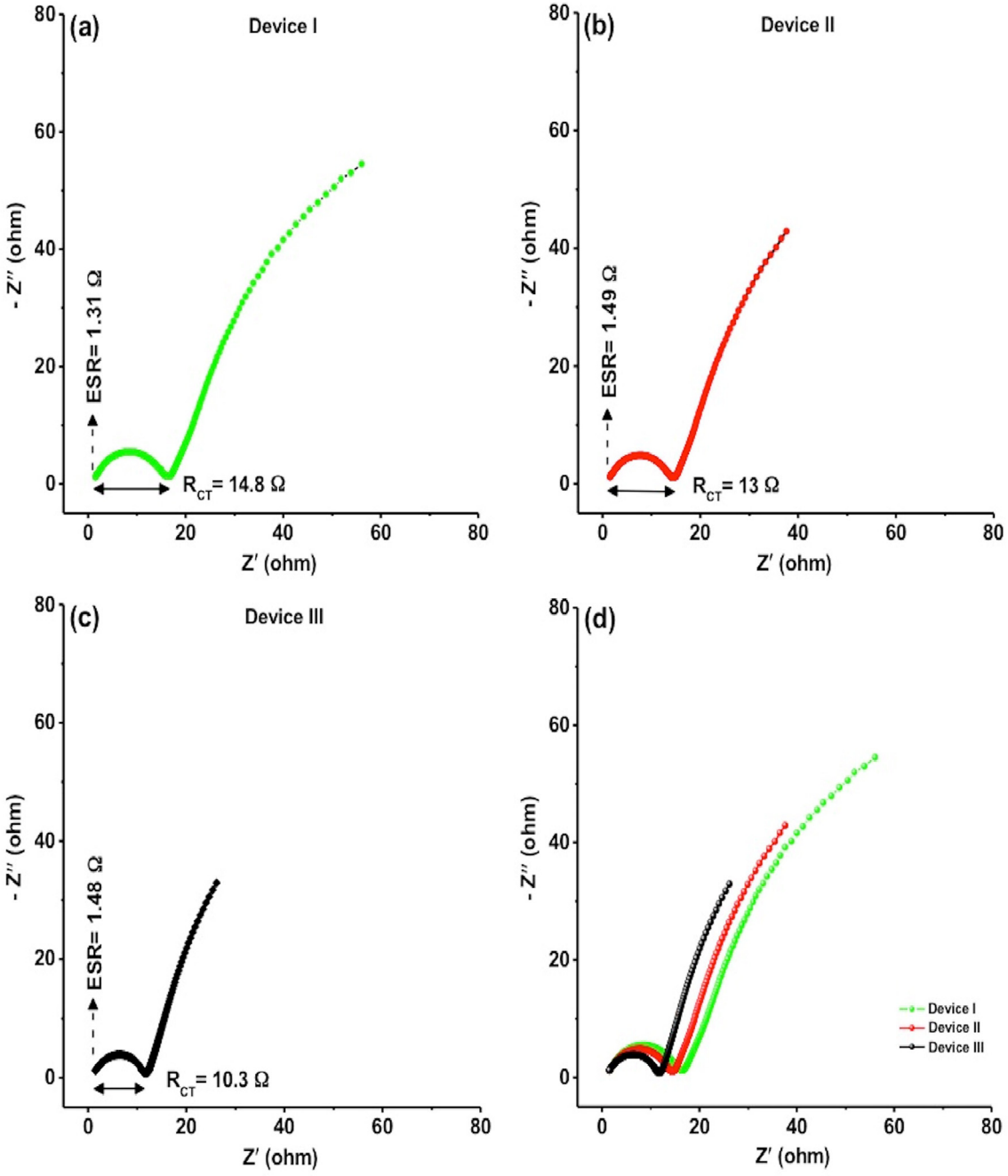


**Fig. 10.** Nyquist impedance plots recorded for (a) Device I, (b) Device II, (c) Device III and (d) comparative Nyquist plots of micro-supercapacitor devices.

properties of solid-state micro-supercapacitors. Fig. 10a–c show Nyquist impedance plots recorded for Device I, Device II and Device III at 5 mV rms perturbation amplitude in the frequency range from 10 000–0.01 Hz at 0.0 V DC voltage. As clearly seen from Fig. 10a–c, Nyquist plots mainly consist of two components in the high- and low-frequency regions, where these impedance responses are consistent with an ideal supercapacitive behavior. In the high-frequency region, typical semi-circle patterns describe charge transfer resistance ($R_{CT}$) and equivalent series resistance (ESR) in the redox-active electrodes that compose micro-supercapacitor devices. ESR includes inner resistance of polymeric electroactive material, contact resistance between redox-active material and current collector substrate and ionic resistance of supporting electrolyte. The ESR values were directly measured to be 1.31 Ω, 1.49 Ω and 1.48 Ω for Device I, Device II and Device III, respectively, from the intercepting point of real-impedance axis (x-axis) and starting point of semi-circle pattern. The small ESR values indicate that **PTCB**, **PTCH** and **PTCO** redox-active materials are possessed of acceptable electronic features for practical energy storage applications. On the other side, diameter of semi-circle corresponds to charge transfer resistance ($R_{CT}$) at the interface of electroactive material/ electrolyte. As shown from Fig. 10a–c, Device I ($R_{CT} = 14.8\ \Omega$) and Device II ($R_{CT} = 13\ \Omega$) exhibited semi-circle parts with wider radius compared with that of Device III ($R_{CT} = 10.3\ \Omega$) This semi-circle tendency further confirms that **PTCO** polymeric network has a more suitable three-dimensional structure enabling easier ion transportation and faster charge transfer processes than **PTCB** and **PTCH** redox-active films.

In the low-frequency areas of Nyquist impedance plots, all micro-supercapacitor devices presented straight portions along the imaginary part (- Z″-axis). The straight line, commonly known as Warburg impedance (*W*), enlightens electrolyte diffusion kinetic during charge/discharge process in the redox-active network. As obviously seen in comparative Nyquist plots (Fig. 10d), Device III exhibited not only a shorter Warburg region, but also a more steep curve than those of Device I and Device II in the low-frequency region, meaning lower diffusion resistance and better capacitive performance for Device III. Such apparent difference between Warburg behaviors can be associated to the morphological structure of **PTCO** redox-active materials. **PTCO** polymeric network provided a rapid capacitive double-layer formation compared to **PTCB** and **PTCH** thanks to its more effective diffusion pathways to facilitate ion mobilities.

## 4. Conclusions

Overall, we have successfully prepared novel N-alkyl substituted poly(3,6-dithienylcarbazole)-based conducting polymer derivatives, **PTCB**, **PTCH** and **PTCO**, and systematically investigated their supercapacitive behaviors as redox-active electrode materials in three- and two-electrode test systems. SEM observations revealed that different alkyl pendant group on the conducting polymer backbone created a pronounced effect on the morphological structures of **PTCB**, **PTCH** and **PTCO** polymeric films. With alkyl chain prolongation from butyl- to octyl-, more convenient morphological networks took shape in terms of easier ion mobility or diffusion and more electric charges storage. Gravimetric specific capacitances of 147.7 F $g^{-1}$ for **PTCB,** 218.7 F $g^{-1}$ for **PTCH** and 509.8 F $g^{-1}$ for **PTCO** were achieved at 2.5 mA $cm^{-2}$ current density with good rate capability rates over a broad potential range (1.5 V) in three-electrode cell configuration under ambient conditions. In addition to three-electrode cell configurations, symmetric micro-supercapacitor device applications performed with **PTCB**, **PTCH** and **PTCO** electrodes (Device I, Device II and Device III) resulted in good capacitive performances. Device I, Device II and Device III delivered comparable specific capacitances ($C_{spec} = 70.4–185.5$ F $g^{-1}$), energy densities ($E = 20.3–55$ W h $kg^{-1}$) and power densities ($P = 750–760$ W $kg^{-1}$) to those of many other conducting polymer-based supercapacitors. More importantly, Device I, Device II and Device III micro-supercapacitors exhibited high long-term cycling stabilities with minimum electroactivity loss after 10 000 charge/discharge cycles. In this context, novel redox-active capacitive materials discussed above are possessed of a promising potential to be utilized in different electrochemical energy storage applications. The results of our present study also confirm that design of novel conducting polymer derivatives can be used as an effective strategy to enhance mechanical strenght and long-term cycling performance of redox-active electrodes as well as increasing charge storage capacity. Furthermore, this perspective could be extended to prepare various conducting polymer-based capacitive materials with better supercapacitive performances different from poly(3,6-dithienylcarbazole) structures.

## Acknowledgements

The authors gratefully acknowledge for generously financial support from the Scientific and Technological Research Council of Turkey (TÜBİTAK, Grant No: KBAG-114Z167). D. Yiğit also thanks TÜBİTAK (KBAG-114Z167) for a postdoctoral scholarship. We would like to thank Elif Akhüseyin Yıldız (Ankara University) for SEM observations.

## Appendix A. Supplementary data

Supplementary data related to this article can be found at https://doi.org/10.1016/j.electacta.2018.06.005.

## References

[1] J. Kim, C.E. Song, B. Kim, I. Kang, W.S. Shin, D. Hwang, Thieno[3,2-b]thiophene-Substituted benzo[1,2-b:4,5-b′]dithiophene as a promising building block for low bandgap semiconducting polymers for high-performance single and tandem organic photovoltaic cells, Chem. Mater. 26 (2) (2014) 1234.
[2] P. Kumar, K. Ranjith, S. Gupta, P.C. Ramamurthy, Electrochemical copolymerization of thiophene derivatives; a precursor to photovoltaic devices, Electrochim. Acta 56 (2011) 8184.
[3] J. Pei, W. Yu, J. Ni, Y. Lai, W. Huang, A.J. Heeger, Thiophene-based conjugated polymers for light-emitting Diodes: effect of aryl groups on photoluminescence efficiency and redox behavior, Macromolecules 34 (21) (2001) 7241.
[4] N.S. Kumar, J.A. Clement, A.K. Mohanakrishnan, Synthesis and characterization of benzo[c]thiophene analogs tethered with dibenzo-heterocycles as potential OLEDs, Tetrahedron 65 (2009) 822.
[5] C. Ma, M. Taya, C. Xu, Flexible electrochromic device based on poly (3,4-(2,2-dimethylpropylenedioxy)thiophene), Electrochim. Acta 54 (2008) 598.
[6] A.L. Dyer, M.R. Craig, J.E. Babiarz, K. Kiyak, J.R. Reynolds, Orange and red to transmissive electrochromic polymers based on electron-rich dioxythiophenes, Macromolecules 43 (2010) 4460.
[7] M.M. Durban, P.D. Kazarinoff, C.K. Luscombe, Synthesis and characterization of thiophene-containing naphthalene diimide n-type copolymers for OFET applications, Macromolecules 43 (2010) 6348.
[8] T. Soganci, M. Ak, E. Giziroglu, H.C. Soyleyici, Smart window application of a new hydrazide type SNS derivative, RSC Adv. 6 (2016) 1744.
[9] Y. Tang, F. He, M. Yu, F. Feng, L. An, H. Sun, S. Wang, Y. Li, D. Zhu, A. Reversible, Highly Selective, Fluorescent sensor for mercury(ii) using poly(thiophene)s that contain thymine moieties, Macromol. Rapid Commun. 27 (2006) 389.
[10] R.H. Baughman, Conducting polymer artificial muscles, Synth. Met. 78 (1996) 339.
[11] W.A. Christinellia, R. Gonçalvesb, E.C. Pereirac, Optimization of electrochemical capacitor stability of poly(o- methoxyaniline)-poly(3-thiophene acetic acid) self-assembled films, Electrochim. Acta 196 (2016) 741.
[12] W. Chen, R.B. Rakhi, H.N. Alshareef, Facile synthesis of polyaniline nanotubes using reactive oxide templates for high energy density pseudocapacitors, J. Mater. Chem. A 1 (2013) 3315.
[13] C. Zhao, C. Wang, Z. Yue, K. Shu, G.G. Wallace, Intrinsically stretchable supercapacitors composed of polypyrrole electrodes and highly stretchable gel electrolyte, ACS Appl. Mater. Interfaces 5 (2013) 9008.
[14] K.S. Ryu, Y. Lee, Y. Hong, Y.J. Park, X. Wu, K.M. Kim, M.G. Kang, N. Park, S.H. Chang, Poly(ethylenedioxythiophene) (PEDOT) as polymer electrode in

redox supercapacitor, Electrochim. Acta 50 (2004) 843.
[15] H. Wang, J. Lin, Z.X. Shen, Polyaniline (PANi) based electrode materials for energy storage and conversion, J. Sci.: Adv. Mater. Dev. 1 (2016) 225.
[16] T. Chen, L. Dai, Flexible supercapacitors based on carbon nanomaterials, J. Mater. Chem. A 2 (2014) 10756.
[17] L. Dong, C. Xu, Y. Li, Z. Huang, F. Kang, Q. Yanga, X. Zhaod, Flexible electrodes and supercapacitors for wearable energy storage: a review by category, J. Mater. Chem. A 4 (2016) 4659.
[18] X. Zhang, Z. Lin, B. Chen, S. Sharma, C. Wong, W. Zhangd, Y. Deng, Solid-state, flexible, high strength paper-based supercapacitors, J. Mater. Chem. A 1 (2013) 5835.
[19] G.A. Snook, P. Kao, A.S. Best, Conducting-polymer-based supercapacitor devices and electrodes, J. Power Sources 196 (2011) 1.
[20] J. Yang, Y. Liu, S. Liu, L. Li, C. Zhang, T. Liu, Conducting polymer composites: material synthesis and applications in electrochemical capacitive energy storage, Mater. Chem. Front 1 (2017) 251.
[21] M. Pumera, The electrochemistry of carbon nanotubes: fundam entals and applications, Chem. Eur J. 15 (2009) 4970.
[22] T. Chen, L. Dai, Carbon nanomaterials for high performance supercapacitors, Mater. Today 16 (7–8) (2013) 272.
[23] R.R. Salunkhe, Y. Lee, K. Chang, J. Li, P.Y. Yamauchi, Nanoarchitectured graphene-based supercapacitors for next-generation energy-storage applications, Chem. Eur J. 20 (2014) 13838.
[24] J. Zhang, J. Xu, D. Zhangz, A structural supercapacitor based on graphene and hardened cement paste, J. Electrochem. Soc. 163 (3) (2016) E83.
[25] C. Ma, Y. Yu, Y. Li, J. Shi, Y. Song, L. Liub, Ion accumulation and diffusion behavior in micro-/meso-pores of carbon nanofibers, J. Electrochem. Soc. 161 (9) (2014) A1330.
[26] S.M. Jung, D.L. Mafra, C. Lin, H.Y. Jung, J. Kong, Controlled porous structures of graphene aerogels and their effect on supercapacitor performance, Nanoscale 7 (2015) 4386.
[27] H. Zhou, Y. Zhang, Electrochemically self-doped TiO2 nanotube arrays for supercapacitors, J. Phys. Chem. C 118 (2014) 5626.
[28] T. Brousse, M. Toupin, R. Dugas, L. Athouël, O. Crosnier, D. Bélangerb, Crystalline MnO2 as possible alternatives to amorphous compounds in electrochemical supercapacitors, J. Electrochem. Soc. 153 (2006) A2171.
[29] Y. Liu, Y. Jiao, Z. Zhang, F. Qu, A. Umar, X. Wu, Hierarchical SnO2 nanostructures made of intermingled ultrathin nanosheets for environmental remediation, smart gas sensor, and supercapacitor applications, ACS Appl. Mater. Interfaces 6 (3) (2014) 2174.
[30] H. Xia, Y.S. Meng, G. Yuan, C. Cui, L. Lu, A symmetric $RuO_2/RuO_2$ supercapacitor operating at 1.6 V by using a neutral aqueous electrolyte, electrochem, Solid State Lett. 15 (4) (2012) A60.
[31] B. Saravanakumar, K.K. Purushothaman, G. Muralidharan, Interconnected V2O5 nanoporous network for high-performance supercapacitors, ACS Appl. Mater. Interfaces 4 (9) (2012) 4484.
[32] C. Yuan, X. Zhang, L. Su, B. Gao, L. Shen, Facile synthesis and self-assembly of hierarchical porous NiO nano/micro spherical superstructures for high performance supercapacitors, J. Mater. Chem. 19 (2009) 5772.
[33] A.G. Pandolfo, A.F. Hollenkamp, Carbon properties and their role in supercapacitors, J. Power Sources 157 (2006) 11.
[34] L.L. Zhang, X.S. Zhao, Carbon-based materials as supercapacitor electrodes, Chem. Soc. Rev. 38 (2009) 2520.
[35] J.F. Mike, J.L. Lutkenhaus, Recent advances in conjugated polymer energy storage, J. Polym. Sci. B Polym. Phys. 51 (2013) 468.
[36] Y. Zhang, H. Feng, X. Wu, L. Wang, A. Zhang, T. Xia, H. Dong, X. Li, L. Zhang, Progress of electrochemical capacitor electrode materials: a review, Int. J. Hydrogen Energy 34 (2009) 4889.
[37] W. Wei, X. Cui, W. Chena, D.G. Ivey, Manganese oxide-based materials as electrochemical supercapacitor electrodes, Chem. Soc. Rev. 40 (2011) 1697.
[38] G. Wang, L. Zhang, J. Zhangb, A review of electrode materials for electrochemical supercapacitors,, Chem. Soc. Rev. 41 (2012) 797.
[39] I. Shown, A. Ganguly, L. Chen, K. Chen, Conducting polymer-based flexible supercapacitor, Energy sci. Eng. 3 (1) (2015) 2.
[40] Y. Huang, H. Li, Z. Wang, M. Zhu, Z. Pei, Q. Xuea, Y. Huang, C. Zhi, Nanostructured polypyrroleasa flexible electrode material of supercapacitor, Nano Energy 22 (2016) 422.
[41] T.M.S.K. Pathiranage, D.S. Dissanayake, C.N. Niermann, Y. Ren, M.C. Biewer, M.C. Stefan, Role of polythiophenes as electroactive materials, J. Polym. Sci. Part A: Polym. Chem. 55 (2017) 3327.
[42] S. Patra, N. Munichandraiah, Supercapacitor studies of electrochemically deposited PEDOT on stainless steel substrate, J. Appl. Polym. Sci. 106 (2007) 1160.
[43] D. Moa, W. Zhoua, X. Maa, J. Xua, D. Zhua, B. Lu, Electrochemical synthesis and capacitance properties of a novelpoly(3,4-ethylenedioxythiophene bis-substituted bithiophene)electrode material, Electrochim. Acta 132 (2014) 67.
[44] D. Mo, W. Zhou, X. Ma, J. Xu, Facile electrochemical polymerization of 2-(thiophen-2-yl)furan and the enhanced capacitance properties of its polymer in acetonitrile electrolyte containing boron trifluoride diethyl etherate, Electrochim. Acta 155 (2015) 29.
[45] W. Zhou, J. Xu, High-operating-voltage all-solid-state symmetrical supercapacitors based on poly(3,4-ethylenedioxythiophene)/poly(-styrenesulfonate) films treated by organic solvents, Electrochim. Acta 222 (2016) 1895.
[46] D. Yigit, M. Gullu, T. Yumak, A. Sınag, Heterostructured poly(3,6-dithien-2-yl-9Hcarbazol- 9-yl acetic acid)/TiO2 nanoparticles composite redox-active materials as both anode and cathode for high-performance symmetric supercapacitor applications, J. Mater. Chem. A 2 (2014) 6512.
[47] D. Yigit, M. Gullu, N-Substituted poly(3,6-dithienylcarbazole) derivatives: a new class of redox-active electrode materials for high-performance flexible solid-state pseudocapacitors, J. Mater. Chem. A 5 (2017) 609.
[48] E. Frackowiak, V. Khomenko, K. Jurewicz, K. Lota, F. Beguin, Supercapacitors based on conducting polymers/nanotubes composites, J. Power Sources 153 (2006) 413.
[49] K. Lotaa, V. Khomenkob, E. Frackowiak, Capacitance properties of poly(3,4-ethylenedioxythiophene)/carbon nanotubes composites, J. Phys. Chem. Solid. 65 (2004) 295.
[50] D. Zhang, X. Zhanga, Y. Chena, P. Yu, C. Wang, Y. Ma, Enhanced capacitance and rate capability of graphene/polypyrrole composite as electrode material for supercapacitors, J. Power Sources 196 (2011) 5990.
[51] Q. Xiao, X. Zhou, The study of multiwalled carbon nanotube deposited with conducting polymer for supercapacitor, Electrochim. Acta 48 (2003) 575.
[52] K. Zhang, L. Zhang, X.S. Zhao, J. Wu, Graphene/polyaniline nanofiber composites as supercapacitor electrodes, Chem. Mater. 22 (2010) 1392.
[53] X. Fu, C. Jia, S. Wu, X. Weng, J. Xie, L. Deng, Electrosynthesis and characterization of a novel electrochromic film based on poly (4,4_-di(N-carbazolyl) triphenylamine), Synth. Met. 188 (2014) 104.
[54] J.Y. Lim, H.C. Ko, H. Lee, Single- and dual-type electrochromic devices based on polycarbazole derivative bearing pendent viologen, Syntax 156 (2006) 695.
[55] D. Yigit, M. Aykan, M. Güllü, Substituent Effect on Supercapacitive Performances of Conducting Polymer-Based Redox Electrodes: poly(3',4'-bis(alkyloxy) 2,2':5',2'-terthiophene) Derivatives, J. Polym. Sci. Part A: Polym. Chem. (2017), https://doi.org/10.1002/pola.28927.
[56] D. Yiğit, S.O. Hacioglu, M. Güllü, L. Toppare, Synthesis and spectroelectrochemical characterization of multi-colored novel poly(3,6-dithienylcarbazole) derivatives containing azobenzene and coumarin chromophore units, Electrochim. Acta 196 (2016) 140.
[57] J. Roncali, R. Garreau, A. Yassar, P. Marque, F. Garnier, M. Lemaire, Effects of steric factors on the electrosynthesis and properties of conducting poly(3-alkylthiophenes), J. Phys. Chem. 91 (27) (1987) 6706.
[58] J. Roncali, A. Gorgues, M. Jubault, Effects of substitution of the median thiophene ring on the electrodeposition and structure of poly(terthienyls), Chem. Mater. 5 (10) (1993) 1456.
[59] I. Namal, A.C. Ozelcaglayan, Y.A. Udum, L. Toppare, Synthesis and electrochemical characterization of fluorene and benzimidazole containing novel conjugated polymers: effect of alkyl chain length on electrochemical properties, Eur. Polym. J. 49 (2013) 3181.
[60] D. Mo, S. Zhen, J. Xu, W. Zhou, B. Lu, G. Zhang, Z. Wang, S. Zhang, Z. Feng, Alkyl chain engineering in the hybrid bithiophene-3,4-ethylenedioxythiophene: synthesis, electronic properties, and electropolymerization, Synth. Met. 198 (2014) 19.
[61] H. Zhang, L. Hu, J. Tu, S. Jiao, Electrochemically assembling of polythiophene film in ionic liquids (ILs) microemulsions and its application in an electrochemical capacitor, Electrochim. Acta 120 (2014) 122.
[62] Y. Huang, J. Tao, W. Meng, M. Zhu, Y. Huang, Y. Fu, Y. Gao, C. Zhi, Super-high rate stretchable polypyrrole-based supercapacitors with excellent cycling stability, Nano Energy 11 (2015) 518.
[63] P. Sivaraman, S.K. Rath, V.R. Hande, A.P. Thakur, M. Patri, A.B. Samui, All-solid-supercapacitor based on polyaniline and sulfonated polymers, Synth. Met. 156 (2006) 1057.
[64] M. Mastragostino, C. Arbizzani, F. Soavi, Conducting polymers as electrode materials in supercapacitors, Solid State Ionics 148 (2002) 493.
[65] C. Arbizzani, M.C. Gallazzi, M. Mastragostino, M. Rossi, F. Soavi, Capacitance and cycling stability of poly(alkoxythiophene) derivative electrodes, Electrochem. Commun. 3 (2001) 16.
[66] E. Ermis, D. Yigit, M. Güllü, Synthesis of poly(N-alkyl-3,4-dihydrothieno[3,4-b][1,4]oxazine) derivatives and investigation of their supercapacitive performances for charge storage applications, Electrochim. Acta 90 (2013) 623.
[67] T. Liu, L. Finn, M. Yu, H. Wang, T. Zhai, X. Lu, Y. Tong, Y. Li, Polyaniline and polypyrrole pseudocapacitor electrodes with excellent cycling stability, Nano Lett. 14 (2014) 2522.
[68] B. Yue, C. Wang, P. Wagner, Y. Yang, X. Ding, D.L. Officer, G.G. Wallace, Electrodeposition of pyrrole and 3-(4-tert-butylphenyl)thiophene copolymer for supercapacitor applications, Synth. Met. 162 (2012) 2216.
[69] D.Y. Liu, J.R. Reynolds, Dioxythiophene-based polymer electrodes for supercapacitor modules, ACS Appl. Mater. Interfaces 2 (2010) 3586.